Utilizing the MODIS 1.38 μm channel for cirrus cloud optical thickness retrievals: Algorithm and retrieval uncertainties

Kerry Meyer[1,2,3] and Steven Platnick[3]

Received 6 August 2010; revised 12 October 2010; accepted 20 October 2010; published 18 December 2010.

[1] The cloud products from the Moderate Resolution Imaging Spectroradiometers (MODIS) on Terra and Aqua have been widely used within the atmospheric research community. The retrieval algorithms, however, oftentimes have difficulty detecting and retrieving thin cirrus, due to sensitivities to surface reflectance. Conversely, the 1.38 μm channel, located within a strong water vapor absorption band, is quite useful for detecting thin cirrus clouds since the signal from the surface can be blocked or substantially attenuated by the absorption of atmospheric water vapor below cirrus. This channel, however, suffers from nonnegligible attenuation due to the water vapor located above and within the cloud layer. Here we provide details of a new technique pairing the 1.38 μm and 1.24 μm channels to estimate the above/in-cloud water vapor attenuation and to subsequently retrieve thin cirrus optical thickness (τ) from attenuation-corrected 1.38 μm reflectance measurements. In selected oceanic cases, this approach is found to increase cirrus retrievals by up to 38% over MOD06. For these cases, baseline 1.38 μm retrieval uncertainties are estimated to be between 15 and 20% for moderately thick cirrus ($\tau > 1$), with the largest error source being the unknown cloud effective particle radius, which is not retrieved with the described technique. Uncertainties increase to around 90% for the thinnest clouds ($\tau < 0.5$) where instrument and surface uncertainties dominate.

Citation: Meyer, K., and S. Platnick (2010), Utilizing the MODIS 1.38 μm channel for cirrus cloud optical thickness retrievals: Algorithm and retrieval uncertainties, *J. Geophys. Res.*, *115*, D24209, doi:10.1029/2010JD014872.

1. Introduction

[2] Clouds have for some time been identified as a significant source of uncertainty in atmospheric and climate research. As such, there have been substantial efforts in recent years to better determine cloud optical and microphysical properties (e.g., optical thickness, effective particle radius, and water path) from satellite [*Buriez et al.*, 1997; *Sherwood*, 2002; *Kahn et al.*, 2008; *Austin et al.*, 2009; *Winker et al.*, 2009], aircraft [*Baum et al.*, 2000; *Jensen and Pfister*, 2005], and ground-based platforms [*Mace et al.*, 2005]. Such efforts are of great importance, particularly for characterizing cloud radiative properties and, ultimately, estimating cloud radiative effects, which are a function of both optical thickness and effective particle size [*Schmidt et al.*, 2007, 2009; *Oreopoulos et al.*, 2009].

[3] Over the past 10 years, data from MODIS on board the Terra and Aqua satellites have proven useful for global studies of cloud properties at high spatial scales. Specifically, the MODIS Level-2 cloud optical and microphysical retrieval algorithm, designated MOD06 and MYD06 for MODIS Terra and Aqua, respectively, [*Platnick et al.*, 2003; *King et al.*, 2010; *Wind et al.*, 2010; *King et al.*, 1998, 2006] provides, among other parameters, cloud optical thickness and effective particle radius at the pixel-level scale (1km at nadir), with aggregation to a global 1° scale in the Level-3 product (MOD08/MYD08). It is known, however, that MOD06 (for simplicity, further references to MOD06 will include MYD06 as the algorithms for Terra and Aqua are the same), and in many instances the MODIS cloud mask (MOD35), often fail for cases of thin cirrus [*Dessler and Yang*, 2003; *Ackerman et al.*, 2008; *Holz et al.*, 2008; *Lee et al.*, 2009]. This is due in part to the fact that passive sensors, such as MODIS, oftentimes find it difficult to distinguish the relatively small signal of thin cirrus from background surface effects, specifically in the visible through shortwave infrared wavelengths used for MOD06 optical property retrievals. This surface sensitivity, however, is drastically reduced, if not completely eliminated, in the 1.38 μm channel (MODIS band 26). The 1.38 μm channel is located within a strong water vapor absorption band; thus, with adequate column water vapor amount, any solar radiation not reflected by high-altitude clouds (e.g., cirrus) can be completely absorbed by the underlying atmosphere. This absorption acts to effectively screen lower clouds and the surface. These unique characteristics enable thin cirrus cloud detection using reflectance measurements at 1.38 μm [*Gao et al.*, 1993].

[4] Previous studies have demonstrated the utility of the 1.38 μm channel for thin cirrus detection [*Gao et al.*, 2002;

[1]Oak Ridge Associated Universities, Oak Ridge, Tennessee, USA.
[2]Goddard Earth Science and Technology Center, University of Maryland Baltimore County, Baltimore, Maryland, USA.
[3]NASA Goddard Space Flight Center, Greenbelt, Maryland, USA.

Copyright 2010 by the American Geophysical Union.
0148-0227/10/2010JD014872

Roskovensky and Liou, 2003]. A Terra MODIS analysis by *Dessler and Yang* [2003] found that, over the tropics, thin cirrus clouds were detectable (i.e., optical thickness greater than 0.02) by the 1.38 μm channel in roughly one third of the pixels determined to be clear sky by the MODIS cloud mask in two 3 day periods from December 2000 and June 2001. Likewise, *Lee et al.* [2009], analyzing 1 year of Aqua MODIS 1.38 μm reflectance data from June 2005 through May 2006, found that over 40% of the clear-sky pixels (as determined by the MODIS cloud mask) contain detectible thin cirrus. It should be noted that these studies focused solely on thin cirrus cases in which the cloud mask, which has a detection limit near an optical thickness of approximately 0.3 [*Ackerman et al.*, 2008], determines the scene to be clear sky. For MOD06 cloud optical properties retrievals, which only attempt retrievals for pixels deemed cloudy by the cloud mask, a supplemental 1.38 μm retrieval can potentially add a significant number of thin cirrus retrievals and provide a more complete characterization of global cloud statistics.

[5] It has previously been shown that reflectance measurements at 1.38 μm are useful in quantitatively determining cloud optical thickness [*Meyer et al.*, 2004, 2007]. However, because up to 10% of the atmospheric water vapor may reside above and within the cirrus layer, there exists a nonnegligible attenuation for which the 1.38 μm reflectance must be properly corrected. In those previous studies, this attenuation was accounted for by means of a large-scale empirical approach [*Gao et al.*, 2002], in which 1.38 μm is paired with a visible window channel, namely 0.66 μm, over a large subset of observations. A single scaling factor, used as a proxy for the net water vapor transmittance, is computed from this subset, and is applied at the pixel level using a simple linear interpolation scheme. In the present study, the underlying concepts of this large-scale empirical approach are applied at the pixel level, i.e., computing independent scaling factors at each pixel. This has several advantages over the large-scale approach, including enabling pixel-level estimates of retrieval uncertainty. It should be noted, however, that the 1.38 μm channel exhibits some sensitivity to cloud microphysics, a result of slight absorption by ice crystals at this wavelength [*Kou et al.*, 1993; *Yang et al.*, 2000]. Consequently, because the 1.38 μm retrieval is intended for cases in which MOD06 fails, and thus no a priori microphysics information is available, assumptions regarding effective particle size distributions are required, which may adversely affect retrieval uncertainties. Furthermore, for drier atmospheres (e.g., column precipitable water approximately less than about 0.5 cm), contamination by lower clouds or the surface is problematic, yet can potentially be alleviated through various screening methods (such as setting thresholds on column precipitable water or top-of-atmosphere to surface two-way path transmittance).

[6] Subsequently a research-level algorithm has been developed that pairs the 1.38 μm channel with the non-absorbing 1.24 μm window channel (MODIS band 5) to estimate the above and in-cloud water vapor attenuation on a pixel-level basis, from which the 1.38 μm reflectance can be corrected and cirrus optical thickness derived. In section 2, cirrus detection using the 1.38 μm channel is discussed. In particular, the methods for estimating the above-cloud water vapor attenuation, the optical thickness retrieval methodology, and retrieval uncertainty estimation will be detailed. In section 3, two case studies will be presented to illustrate the capability of the new 1.38 μm retrieval. Section 4 describes the estimation of retrieval uncertainty. Finally, the summary and conclusions are discussed in section 5.

2. Cirrus Detection With 1.38 μm

[7] Because the 1.38 μm channel is quite sensitive to thin cirrus (and, in turn, cirrus optical thickness), it can potentially be used to retrieve properties for clouds that otherwise would have been missed by MOD35 and MOD06. The utility of this channel is illustrated in Figure 1. Figure 1a shows the true color RGB image of a Terra MODIS granule taken over South America on 21 October 2007 (1400 UTC). Focus on the region of cirrus "fingers" over southern Brazil, bounded by the red box (upper right). The cloud mask product (MOD35) is shown in Figure 1b. Comparing MOD35 to the pixels with measurable 1.38 μm reflectance in Figure 1c, it is quite evident that, in this case, the cloud products miss possible thin cirrus. This is further illustrated in Figure 1d, a plot of the extent of MOD06 cloud retrievals (red) along with potential additional thin cirrus detection from 1.38 μm (green). Note here that the 1.38 μm observations have been screened using the MODIS reflectance uncertainty indexes (UI) provided within the MODIS Level-1b calibrated radiance/reflectance files for data reliability. The MODIS UI, consisting of integers ranging from 0 to 15, is computed from the pixel-level radiometric uncertainties (and thus can be scaled back to relative uncertainty in percent of reflectance), with 0 (15) representing the smallest (largest) uncertainties. Typically, pixels with a UI of 15 are unusable, and should be discarded [*Xiong et al.*, 2005].

[8] Despite the evident thin cirrus detection capabilities of the 1.38 μm channel, and the potential for improving MOD06 with supplemental optical thickness retrievals, a significant obstacle remains. In particular, quantifying and correcting for the above and in-cloud water vapor attenuation at 1.38 μm. Two approaches to this problem are detailed below, namely, the large-scale "cirrus reflectance" approach, and the new pixel-level approach. A brief discussion of the thin cirrus cloud optical thickness retrieval methodology follows.

2.1. The "Cirrus Reflectance" Approach

[9] Assuming a homogeneous thin cirrus cloud layer located above a "virtual surface" (the cumulative effects of surface, low cloud, aerosol reflectance, and molecular scattering), the reflectance $R(\lambda)$ measured by a satellite sensor at wavelength λ can be written in simplified form, omitting zenith (μ, μ_0) and azimuth (ϕ, ϕ_0) dependencies for simplicity, as [*Gao et al.*, 2002]

$$R(\lambda) = T_w R_c(\lambda) + T_w R_{vs}(\lambda), \tag{1}$$

where $R_c(\lambda)$ is the reflectance of the cirrus cloud, T_w is the two-way water vapor transmittance above and within the cloud, and $R_{vs}(\lambda)$ is the reflectance contribution of the "virtual surface" (note that this term accounts for the virtual surface albedo, as well as the downward and upwelling

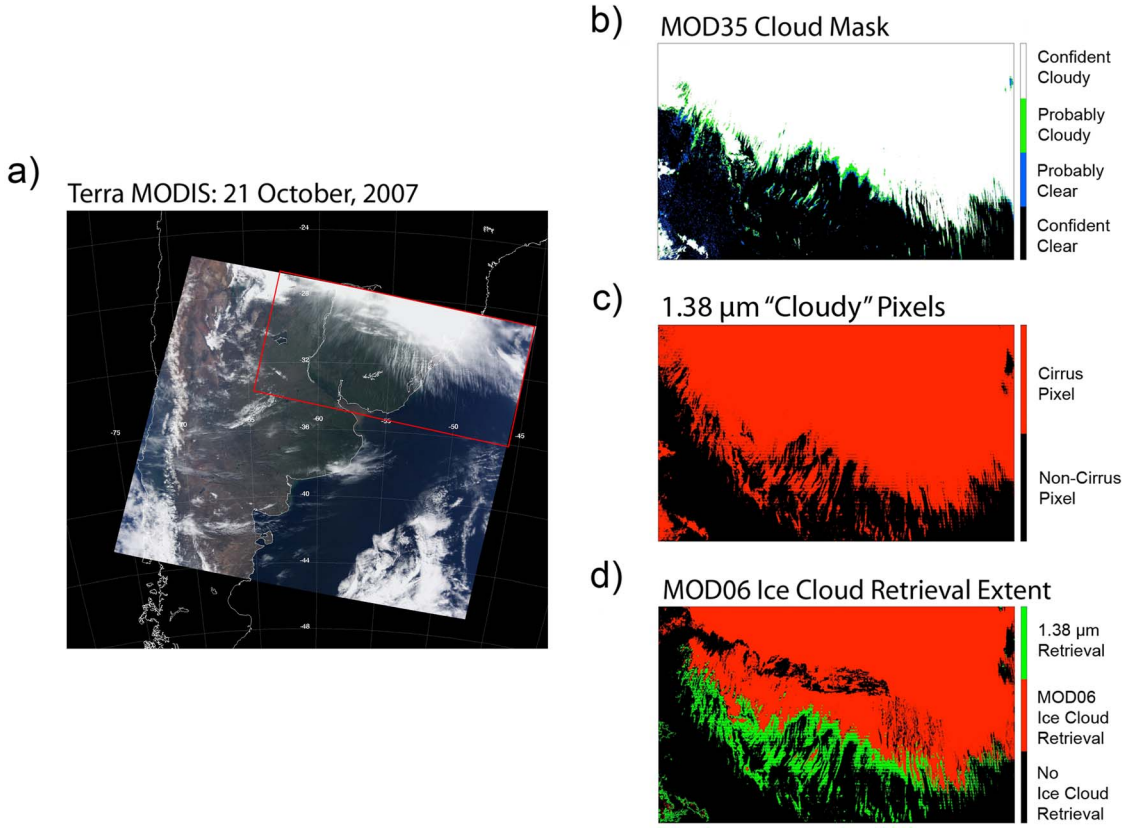

Figure 1. Cirrus detection with the 1.38 μm channel. (a) RGB for Terra MODIS granule taken on 21 October 2007 (1400 UTC). (b) MOD35 cloud mask for region bound by red box in Figure 1a. (c) "Cloudy" pixels determined from measureable 1.38 μm reflectance. (d) Pixels with a successful MOD06 ice cloud optical thickness retrieval (red), with potential additional thin cirrus retrievals from the 1.38 μm channel (green).

diffused transmittances of the cloud). If at λ = 1.38 μm, because of its location in a strong water vapor absorption band, R_{vs} becomes zero (complete absorption by the water vapor below the cirrus layer), then equation (1) further simplifies to

$$R(1.38\mu m) = T_w R_c(1.38\mu m). \tag{2}$$

[10] Furthermore, it has been found that, for reflectance due to cirrus clouds in a transparent atmosphere with no surface reflection, there is a linear relationship between 1.38 μm and channels between 0.4 and 1.0 μm [*Gao et al.*, 1998]. Specifically,

$$R_c(1.38\mu m) = aR_c(0.4 < \lambda < 1.0\mu m), \tag{3}$$

where R_c(1.38 μm) and R_c(0.4 < λ < 1.0 μm) are the cirrus cloud reflectances at 1.38 μm and a channel between 0.4 and 1.0 μm, respectively, and a is a scale factor (smaller than 1.0) required to account for weak ice crystal absorption at 1.38 μm [*Gao et al.*, 1998]. In practice, it is assumed that a ≈ 1 (i.e., near 1-to-1 relationship in equation (3)), and is held constant for all retrievals.

[11] Inserting equation (3) into equation (2) yields the basic equation for cirrus reflectance in the spectral region between 0.4–1.0 μm, namely,

$$R_c(0.4 < \lambda < 1.0\mu m) = \frac{1}{\Gamma} R(1.38\mu m), \tag{4a}$$

where

$$\Gamma = T_w a \tag{4b}$$

This effectively reduces the equation to one unknown, since R(1.38 μm) is a measured quantity [*Gao et al.*, 2002].

[12] In the cirrus reflectance approach, the parameter Γ in equation (4b) is derived using a bispectral scatterplot technique pairing 1.38 μm with a visible channel (in practice 0.66 μm). A given scene obtained from satellite observations, here a granule of MODIS data, is divided evenly into 16 subscenes, or subgranules. The value of Γ for each subgranule is determined from the slope of the R(1.38 μm) versus R(0.66 μm) scatterplot. This technique is illustrated in Figure 2, a sample granule taken from Terra MODIS on 21 October 2007 at 1400 UTC. Figure 2a shows the true color RGB composite, with red grid lines denoting the 16 subgranules. The reflectance scatterplot of the subgranule

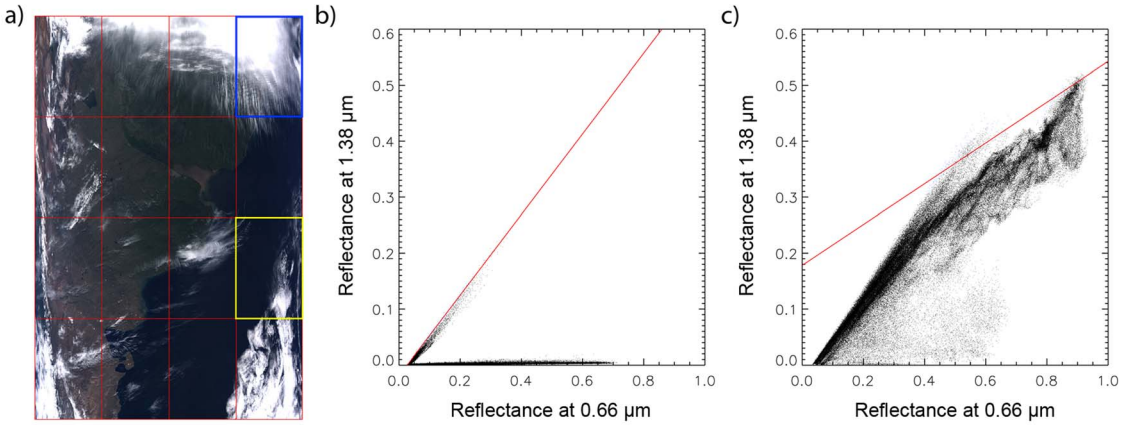

Figure 2. The cirrus reflectance approach. (a) MODIS RGB from Terra on 21 October 2007, with red grid lines denoting subgranule boundaries for slope calculations. (b) Reflectance scatterplot corresponding to the subgranule bounded by the yellow box in Figure 2a, with a red line denoting the calculated slope (Γ). Here ice cloud pixels are those closely clustered around the red line; lower water cloud pixels are clustered near the bottom of the plot. (c) Scatterplot corresponding to the complex subgranule bounded by the blue box in Figure 2a, illustrating the limitations of the large-scale empirical cirrus reflectance approach.

highlighted in yellow is shown in Figure 2b. Here the slope of the red line is the Γ parameter. To avoid a "chessboard" effect resulting from granule subdivision, a weighted interpolation scheme is used to approximate Γ at pixel level from the surrounding subgranule values of Γ [*Gao et al.*, 2002]. The resulting visible cirrus reflectance can then be converted, by means of a precalculated look-up library, to cirrus cloud optical thickness [*Meyer et al.*, 2004, 2007].

[13] It has become evident, however, that, while the cirrus reflectance method is useful for general cirrus/high cloud applications, the applicability of the approach for thin cirrus optical thickness retrievals can be quite limited. For instance, Figure 2b illustrates an ideal case, with a clear delineation between ice clouds (the pixels tightly clustered near the red line) and the underlying surface and low-level water clouds (the pixels near the bottom of Figure 2b). Introducing complexity (e.g., varying cloud heights, thicknesses and particle effective sizes, multilayer clouds) into the subgranule, such as that shown in Figure 2c (corresponding to the blue highlighted subgranule in Figure 2a), introduces a number of issues that inhibit the cirrus reflectance approach. First, it is evident that the Γ value calculated for this subgranule (shown as the red line) is highly influenced by the thicker clouds, and thus provides little information for thin cirrus (note that adjustments to various thresholds can potentially alleviate this problem). Second, forward radiative transfer (RT) calculations have shown that the scale factor a in equation (4b) is dependent on effective particle size (and to a much lesser extent on optical thickness, which is discussed below in section 2.3). Thus, Γ may not provide sufficient information about the pixel-level water vapor attenuation for subgranules in which particle size varies widely. In light of this size sensitivity, the assumption of a near 1-to-1 linear relationship between 1.38 and 0.66 μm cirrus cloud reflectance is problematic. Third, and perhaps most important in terms of retrieval development, pixel-level retrieval uncertainties, accounting for uncertainty components such as sensor calibration and effective size sensitivity, are difficult to estimate for a large-scale statistical technique such as the cirrus reflectance approach. It is therefore necessary to develop an alternate approach to estimate the above and in-cloud water vapor attenuation at 1.38 μm.

[14] Closer examination of the scatterplot in Figure 2b reveals a potential solution. Intuitively, as cloudy pixels become more optically thin (i.e., reflectance decreases), the scatterplot converges to the clear-sky reflectance at both wavelengths. Indeed, in Figure 2b the plot converges to a 0.66 μm reflectance of roughly 0.025, a value characteristic of direct solar illumination of an ocean surface away from the Sun glint region (note that in this case, 1.38 μm converges to zero, a result of complete absorption by the underlying atmospheric water vapor for the granule being considered). Assuming that the clear-sky window channel reflectance for each cloudy pixel can be estimated with a specified uncertainty, it therefore becomes possible to, in turn, estimate above/in-cloud water vapor transmittance for the 1.38 μm signal on a pixel-level basis.

2.2. The Pixel-Level 1.38 μm Approach

[15] Subsequently, a new bispectral technique (hereafter referred to as the 1.38 μm retrieval) has been developed to estimate the above and in-cloud water vapor attenuation at pixel level using the 1.38 μm channel and a visible or shortwave infrared window channel. Conceptually, this approach contains implicit assumptions similar to the cirrus reflectance approach (namely, thin optical thickness convergence to the clear-sky reflectance). For a given thin cirrus cloudy pixel, the clear-sky reflectance at the selected window channel is estimated from an assumed (or modeled) spectral surface reflectance and ancillary atmospheric profile. A slope, Γ, is then calculated from the estimated clear-

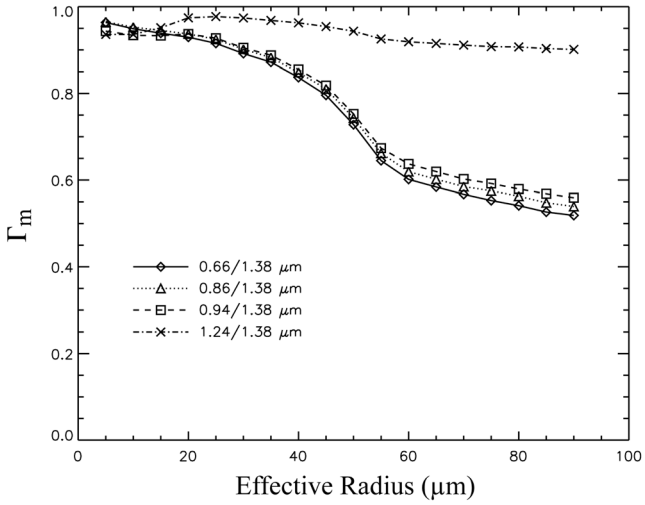

Figure 3. Modeled scaling factor (Γ_m) dependence on ice particle effective size, assuming a surface diffuse albedo of 5%, for the four wavelengths considered for 1.38 μm water vapor transmittance estimation. Due to close spectral proximity (and hence similar ice cloud bulk-scattering properties), the 1.24/1.38 μm pair minimize slope dependence on effective size.

sky and observed cloudy reflectances (similar in concept to the red line in Figure 2b, drawn through each observed cloudy pixel reflectance pair), such that

$$\Gamma = \frac{R(1.38\mu m)}{R(window) - R_{clr}(window)}, \tag{5}$$

where $R(1.38\mu\text{m})$ and $R(window)$ are the measured 1.38 μm and window channel reflectances, respectively, and $R_{clr}(window)$ is the estimated clear-sky window channel reflectance (itself a function of the window channel surface albedo and slight atmospheric attenuation or scattering (e.g., aerosols), and molecular scattering).

[16] Under the near-linear 1-to-1 assumptions of *Gao et al.* [2002], the slope Γ would be the estimated transmittance proxy. However, because this assumption does not account for the effective particle size sensitivity of Γ, a size-dependent scaling factor (Γ_m, similar in function to the scale factor a in equation (3)) must be introduced. This scaling factor, however, cannot be provided by observations, but must be obtained from forward RT calculations. In practice, this can be accomplished with a standard 1D RT code, for example, the discrete ordinates radiative transfer (DISORT) method [*Stamnes et al.*, 1988], coupled with ice cloud bulk scattering property models. Here the ice models developed for the MOD06 Collection 5 processing stream [*Baum et al.*, 2005a, 2005b] are used. Cirrus cloud reflectances for a range of effective radii and optical thicknesses within a transparent atmosphere, and over a surface with specified window channel reflectance, are then calculated. Thus

$$\Gamma_m(\tau, re) = \frac{R_m(1.38\mu m, \tau, re)}{R_m(window, \tau, re) - R_{clr}(window)}, \tag{6}$$

where $R_m(1.38\mu\text{m},\tau,re)$ and $R_m(window,\tau,re)$ are the modeled 1.38 μm and window channel reflectances, respectively, for a cirrus cloud with optical thickness τ and effective radius re. The above/in-cloud two-way water vapor transmittance at 1.38 μm (T_w) can then be estimated in a manner similar to equation (4b), such that:

$$T_w = \Gamma / \Gamma_m. \tag{7}$$

Finally, inserting equation (7) into equation (2) yields the corrected 1.38 μm reflectance, $R_c(1.38\mu\text{m})$.

[17] Because 1.38 μm is somewhat sensitive to the cloud microphysics, and there is no a priori effective size information for pixels lacking MOD06 retrievals, it is desirable to reduce the sensitivity to effective particle size. In Figure 3, modeled scaling factor values (Γ_m), calculated assuming a surface diffuse albedo of 5%, are plotted versus ice particle effective radius (r_e) for four band combinations (0.66/1.38 μm, 0.86/1.38 μm, 0.94/1.38 μm, and 1.24/1.38 μm). It is quite evident from Figure 3 that the 1.24/1.38 μm channel combination (dash-dotted line) exhibits a remarkable minimization to the size sensitivity. This is due in large part to the close spectral proximity of the two wavelengths, which results in minimal differences in their respective scattering properties, e.g., single-scattering albedo, ω_0, and asymmetry parameter, g. Note that the size sensitivities of the other band combinations result from differences in ω_0 between 1.38 μm and 0.66, 0.86, and 0.94 μm (the bulk scattering properties at both 1.24 μm and 1.38 μm have smaller ω_0 due to ice crystal absorption, which intensifies with increasing particle size).

[18] Furthermore, Figure 4 shows that the 1.24/1.38 μm channel combination (again the dash-dotted line) minimizes the uncertainty and bias of the estimated above/in-cloud water vapor transmittance. Here simulated satellite-measured reflectances are calculated for a variety of single-layer cirrus cloud scenarios, assuming a cloudy tropical ocean atmospheric profile [*Wind et al.*, 2010]. For the RT calculations, the absorption of atmospheric gases is accounted for using the correlated-k routines of *Kratz* [1995]. Specifically, the cirrus scenarios include combinations of three cloud physical thicknesses (1, 2, 3 km), four cloud top heights (12, 13, 14, 15 km), nine ice effective particle radii (10 to 50 μm), 13 optical thicknesses (0.1 to 20.0), and 12 view geometries (selected to represent a typical tropical ocean MODIS granule). The above/in-cloud water vapor transmittance for each scenario is then estimated with the pixel-level approach, and the error (relative to the actual transmittance) is then determined. It is clear that, by minimizing the size sensitivity, as well as the uncertainty and bias of the estimated transmittance, the 1.24/1.38 μm combination is the optimal band pairing. In addition, compared to 0.66 μm, and to a lesser extent 0.86 μm, Rayleigh scattering is negligible at 1.24 μm; thus, an additional Rayleigh correction, which can potentially increase retrieval uncertainty, is unnecessary. Consequently, 1.24 μm has been selected as the window channel in equations (4) and (5), and a look-up library of Γ_m values has been constructed for various effective particle radii, surface reflectance, and cloud optical thickness.

2.3. Retrieving Thin Cirrus Cloud Optical Thickness

[19] Once the above/in-cloud water vapor transmittance is estimated, and the measured 1.38 μm reflectance is corrected, the thin cirrus optical thickness can be retrieved

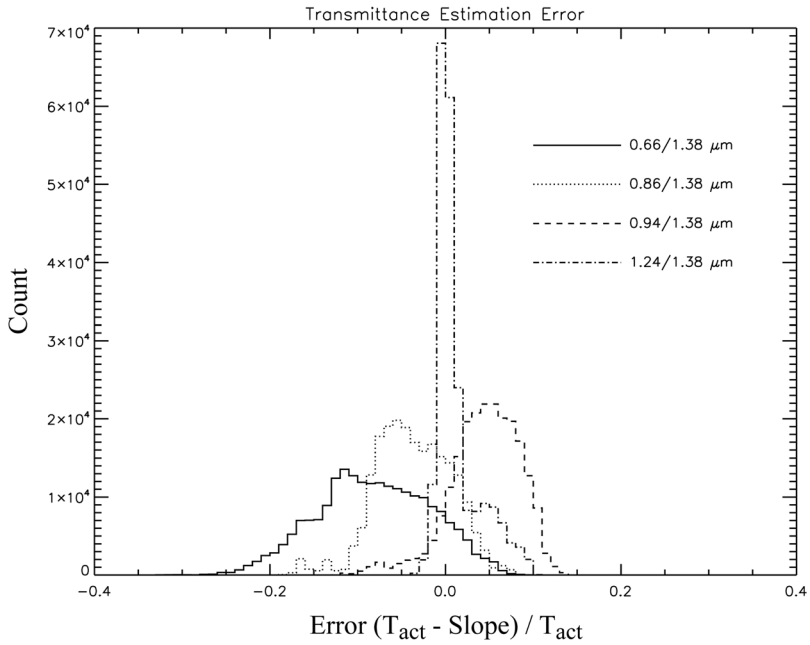

Figure 4. Histogram of relative path transmittance errors estimated from forward RT calculations. Note that the 1.24/1.38 μm combination is centered near zero.

following a straightforward look-up table (LUT) approach. It should be noted here that the present retrieval in fact differs from previous efforts [*Meyer et al.*, 2004, 2007], which derived cirrus optical thickness from the conventional "cirrus reflectance" approach based on the pairing of a visible (i.e., 0.66 μm) band with the 1.38 μm band. The look-up tables contain cirrus cloud bidirectional reflectances for 18 particle effective radii (5 to 90 μm), 23 optical thicknesses (0.002 to 100.0), 16 solar and sensor zenith angles (0 to 75°), and 19 relative azimuth angles (0 to 180°). The bidirectional reflectance LUTs are generated from the MOD06 Collection 5 ice models [*Baum et al.*, 2005a, 2005b] under the assumption of a cirrus cloud located within a transparent atmosphere over a nonreflecting surface. It is known that ice crystal microphysics can vary with changing cloud characteristics such as age, thickness and location, and thus thin cirrus clouds may not be ideally represented by the MOD06 Collection 5 ice models; nevertheless, these models are chosen such that the 1.38 μm approach remains consistent with MOD06. In addition, because the 1.38 μm channel is sensitive to particle effective size, and no a priori size information is available for thin cirrus not retrieved by MOD06, a single size is assumed for all retrievals. Here an effective radius of 30 μm is assumed, which roughly corresponds to the mode of the global distribution of Aqua MODIS effective radius retrievals (this is also consistent with the assumption made for MOD06 "partial" retrievals, i.e., pixels that fail to find a physical effective radius within the look-up table space). The complete retrieval algorithm (including water vapor transmittance estimation) has subsequently been integrated within a research-level MOD06 code.

[20] The pixel-level water vapor transmittance estimation requires ancillary information, such as surface albedo, atmospheric profile, etc., for calculating both Γ and Γ_m. At present, retrievals are restricted to ocean cases, where atmospheric water vapor content is large, and also cases where the surface is relatively dark at 1.24 μm. For ocean cases, the surface albedo can be defined one of two ways. One is to assume a Lambertian surface (i.e., angular independence) with a fixed albedo. This is the assumption used in the current MOD06 algorithm, in which the ocean albedo is fixed at 5%, a value typical of the surface under diffuse illumination. Yet this assumption can be problematic, particularly for thin cirrus. For moderately thick clouds, the diffuse component dominates; as cloud optical thickness decreases, however, the direct component gains importance, eventually dominating for very thin clouds. Because the 1.38 μm retrieval is intended mainly for failed MOD06 retrievals, presumably with very thin cirrus, it is critical to assume an appropriate surface albedo at 1.24 μm. Here the albedo is estimated using a Cox-Munk approach [*Cox and Munk*, 1954a, 1954b] for calculating the ocean surface bidirectional reflectance distribution function (BRDF). Thus, the angular dependence of ocean surface reflectance under direct illumination can be captured (this is of particular importance over Sun glint regions, where surface reflection can be much higher than the 5% diffuse albedo).

[21] Atmospheric profile information, used to estimate the slight atmospheric attenuation at 1.24 μm, is obtained from the National Centers for Environmental Prediction (NCEP) global model reanalyses. The Cox-Munk approach itself requires additional ancillary information, specifically the wind speed and direction (in addition to the solar/sensor angle information). Wind speed is derived from the component surface winds obtained directly from NCEP reanalyses; for simplicity, wind direction is fixed to the solar angle (i.e., from the direction of the Sun). These ancillary data are obtained through (and most are presently used by) the MOD06 optical property retrieval algorithm.

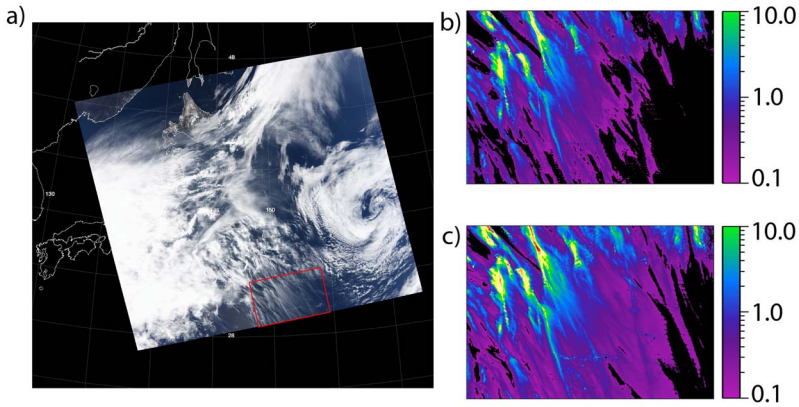

Figure 5. Optical thickness retrievals for the 14 April 2009 case study (0320 UTC). (a) MODIS RGB from Aqua. The red outlined region denotes the area of interest. (b) MOD06 retrieved ice cloud optical thickness. (c) Retrieved optical thickness from the 1.38 μm approach.

[22] Because the estimation of water vapor transmittance (T_w) exhibits a small sensitivity to optical thickness (due primarily to the surface contribution to thin cirrus reflectance at 1.24 μm resulting in Γ_m sensitivity to optical thickness), implementing the retrieval technique requires an iterative approach. First, the data are filtered using the uncertainty index (UI), a pixel-level parameter provided within the MODIS Level-1b data set, to remove expected noisy pixels. A "first guess" optical thickness is then calculated from the measured 1.38 μm reflectance using the single-scatter approximation. Next, the appropriate Γ_{m} is selected corresponding to this optical thickness and estimated surface reflectance, and the above/in-cloud water vapor attenuation at 1.38 μm is estimated. The 1.38 μm reflectance is then corrected and converted to optical thickness via the cirrus bidirectional reflectance LUT. Finally, this optical thickness is compared with the initial guess. If the difference is sufficiently small (for instance, relative difference less than 0.1%), then the retrieval is said to have converged, and this optical thickness is reported as the retrieved value; otherwise, a new Γ_{m} is selected corresponding to the retrieved optical thickness, and the retrieval proceeds until optical thickness converges (typically within 3 to 4 iterations).

[23] Since the 1.38 μm retrieval is limited to cases in which the measured 1.38 μm reflectance is due solely to cirrus clouds, it is important that, prior to any retrieval attempt, each pixel is vigorously screened to establish confidence that there is no surface or low-cloud contamination. Perhaps the most significant screening technique is filtering with the Level-1b UI, such that pixels with large reflectance uncertainty (i.e., UI = 15), and, typically, very small reflectance, are discarded. Because surface contamination often manifests itself as very small 1.38 μm reflectance, UI filtering can in fact remove significant numbers of surface-contaminated pixels. In addition, a second screening technique can be used, in which column two-way path transmittance at 1.38 μm is estimated from the NCEP atmospheric profile; here pixels with nonnegligible transmittance are discarded. It should be noted that further refinement of these and other screening techniques is required before the 1.38 μm approach is applied for global retrievals. In section 3, the applicability of the 1.38 μm approach is illustrated using two case studies.

3. Case Studies

[24] Here two case studies from Aqua MODIS are presented, one off the coast of Japan on 14 April 2009 (0320 UTC), the other over the western Pacific Ocean on 21 October 2009 (0510 UTC). Both cases involve scenes with very thin to moderately thick single-layer cirrus clouds, as well as sufficiently moist atmospheres such that the surface is completely screened at 1.38 μm.

3.1. The 14 April 2009 Case

[25] Figure 5a shows the true color RGB composite for an Aqua MODIS granule off the coast of Japan on 14 April 2009 at 0320 UTC. Here a small region of single-layer cirrus is visible within the red-bounded box at the southern end of the granule. Note the presence of Sun glint in the clear-sky region lying to the west–southwest of the cirrus region. The cirrus clouds are located over the transition zone between the peak Sun glint and the dark ocean, underscoring the importance of having an ocean surface BRDF. Mean column precipitable water for the subregion, taken from the NCEP reanalyses, is 1.3 cm, a sufficiently large value for complete 1.38 μm atmospheric absorption (generally, precipitable water values less than approximately 0.5 cm can result in surface and low-level cloud contamination at 1.38 μm).

[26] The MOD06 (operational retrieval, ocean surface diffuse albedo fixed at 5%) and 1.38 μm ice cloud optical thickness retrievals for the red outlined subregion in Figure 5a are shown in Figures 5b and 5c, respectively. Note here that MOD06 "partial" retrievals, which typically correspond to the thinnest clouds retrieved by MOD06, are included in Figure 5b (such pixels are not included in the global MODIS Level-3 aggregated statistics). It is evident from comparing the two images that the 1.38 μm approach produces a noticeably larger number of thin cirrus retrievals (shown as shades of violet) than does MOD06 (an approximate 38% increase).

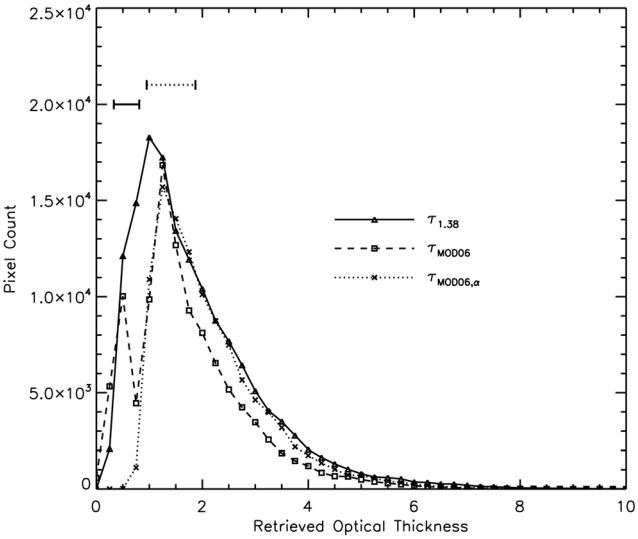

Figure 6. Optical thickness retrieval histograms for the 1.38 μm approach (solid line), operational MOD06 (dashed line), and modified MOD06 (dotted line) for the 14 April 2009 case shown in Figure 5. The modified MOD06 uses the mean Cox-Munk ocean surface albedo (here about 1%). The horizontal solid and dotted lines denote the range of optical thickness retrieved by CALIPSO (Version 3 level 2 5 km Cloud Layer product) and the 1.38 μm approach (nearest pixels to CALIPSO ground track), respectively.

[27] The increased number of retrievals is further illustrated by the histograms of retrieved optical thickness, shown in Figure 6. Here the 1.38 μm and MOD06 retrievals are denoted by the solid and dashed lines, respectively. First, note that the 1.38 μm algorithm produces more retrievals at all optical thicknesses, except within the smallest two optical thickness bins. Also note the double peak in the MOD06 histogram. The secondary peak at smaller optical thicknesses is in fact due to partial retrievals, a result of overestimating the surface albedo (therefore overestimating the surface contribution in the MODIS observations). Fixing the 1.24 μm ocean surface albedo within MOD06 to the mean Cox-Munk BRDF value within the retrieval region (approximately 1%, much smaller than the operational assumption of 5% for diffuse surface illumination) results in a retrieved optical thickness histogram shown as the dotted line in Figure 6. Note here that the MOD06 retrievals have been shifted to larger optical thicknesses, and the secondary peak is removed (in addition, the partial retrievals become full retrievals). Note also that there are currently no aerosol effects in the MOD06 LUTs; MOD06 Collection 6 will, however, include aerosol effects, assuming a $\tau_{aerosol}$ of 0.1 in the marine boundary layer. It is evident that with a presumably more realistic surface albedo estimate, the 1.38 μm approach produces significantly more thin cirrus retrievals.

[28] Also plotted in Figure 6 is the range of optical thickness (i.e., ± 1 standard deviation, centered at the retrieval mean) retrieved by CALIPSO over the subregion, shown as the solid horizontal line, derived from the Version 3 level 2 5 km Cloud Layer product [*Young et al.*, 2008]. Note here that the only retrievals considered are those in which the CALIPSO cloud profiles are not totally attenuated, such that the retrieved optical thickness corresponds to the entire cloud depth. The dotted horizontal line is the 1.38 μm retrieved optical thickness range for the MODIS pixels nearest the CALIPSO ground track that correspond to the non-totally-attenuating CALIPSO cloud profiles. Here the mean of the CALIPSO optical thickness retrievals (72 total pixels) is approximately 0.57, while the MODIS 1.38 μm retrieval mean is much larger, near 1.4.

[29] For this case, the CALIPSO retrieval range lies within both the MOD06 and 1.38 μm retrieval histograms; however, there is no overlap with the 1.38 μm retrieval range near CALIPSO ground track. Both the MODIS and CALIPSO teams are aware of the difference in ice cloud optical thickness retrievals between their respective products. Several hypotheses have been proposed to explain this difference, but a consensus has yet to be reached. The multiple scattering effect is known to have a significant impact on the CALIPSO retrieval, which may partially explain the difference. In addition, uncertainty in ice particle microphysics might also play a role. Several previous studies have shown that roughening of the ice particle surface and internal inclusion of air bubbles reduced the asymmetry factor of ice particles [*Macke et al.*, 1996a, 1996b; *Xie et al.*, 2009], which in turn decreases ice cloud optical thickness retrievals in MOD06; nevertheless, this is still an open question.

[30] Furthermore, of the 72 collocated CALIPSO retrievals, none are constrained. Constrained retrievals use direct measurements of the cloud layer two-way transmittance to derive the lidar ratio (the ratio of extinction to backscatter), whereas in unconstrained retrievals the lidar ratios are assumed constants. Because changes in cloud microphysics can cause varying lidar ratios, constrained retrievals are considered more reliable than unconstrained. Yet the constrained method has uncertainties, as well, which can affect optical thickness retrievals. Undetected aerosol above or below the cloud layer can bias the retrieval results (the constrained method relies on comparing the signal from the above- and below-cloud clear regions). In addition, daytime measurements oftentimes have low signal-to-noise ratios (SNR), resulting in decreased accuracy in the cloud layer two-way transmittance estimate. Although all of these factors are known to affect the retrievals, a definitive explanation of the differences observed between MODIS and CALIPSO optical thickness retrievals is at present unknown and warrants further investigation.

3.2. The 9 August 2009 Case

[31] Figure 7a shows the true color RGB composite for an Aqua MODIS granule over the western Pacific Ocean on 9 August 2009 at 0510 UTC. Here a long band of cirrus clouds associated with Typhoon Morakot (shown making landfall on the coast of China) is visible across the center of the granule. Again, the red bounded box denotes the region of interest. Similar to Figure 5a, this subregion is located over the transition zone between the expected peak Sun glint and the dark ocean, although the Sun glint is not as evident here due to cloud cover and the presence of the islands of Indonesia. Mean column precipitable water for the subregion, taken from the NCEP reanalyses, is 5.2 cm, again a sufficiently large value for complete 1.38 μm absorption.

[32] The MOD06 and 1.38 μm ice cloud optical thickness retrievals for the red outlined subregion in Figure 7a are

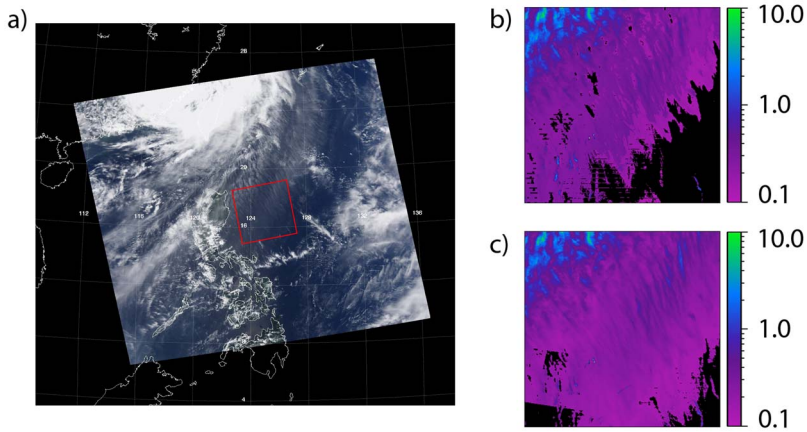

Figure 7. Optical thickness retrievals for the 9 August 2009 case study (0510 UTC). (a) MODIS RGB from Aqua. The red outlined region denotes the area of interest. (b) MOD06 retrieved ice cloud optical thickness. (c) Retrieved optical thickness from the 1.38 μm approach.

shown in Figures 7b and 7c, respectively. MOD06 partial retrievals are included in Figure 7b. Again, it is clear that the 1.38 μm approach produces a larger number of thin cirrus retrievals, particularly at the cloud edges; additional retrievals fill the gaps present in the middle of the cloud field. Note, however, the missing 1.38 μm retrievals present in the lower left corner of Figure 7c, resulting primarily from the coarse NCEP reanalysis grid (1° × 1°). These pixels lie directly over the expected Sun glint peak, while the corresponding NCEP grid cell has wind speed roughly 2–3 m s^{-1} weaker than the surrounding grid cells, and is located partially over land. Thus, the estimated Sun glint is stronger, resulting in surface reflectances larger than the measured cloudy reflectances, negative Γ values, and, ultimately, failed retrievals. Nevertheless, the 1.38 μm approach still retrieves more cirrus than does MOD06 (an approximate 21% increase).

[33] Again, the increased number of retrievals is evident in the retrieval histograms, shown in Figure 8. The 1.38 μm and MOD06 retrievals are denoted by the solid and dashed lines, respectively. Note here that, similar to the 14 April case (Figure 6), the MOD06 distribution exhibits a double peak, although the secondary peak is less well defined. Fixing the 1.24 μm ocean surface albedo to the mean Cox-Munk BRDF value (here approximately 4.6%) results in a distribution shown as the dotted plot. Unlike Figure 6, because the mean Cox-Munk albedo is not significantly different from the assumed Lambertian albedo, this does not significantly shift the distribution; it does, however, remove the small secondary peak while increasing the magnitude of the mode. For both MOD06 scenarios, the 1.38 μm approach produces a larger number of thin cirrus retrievals.

[34] Similar to Figure 6, the range of optical thickness (again, ±1 standard deviation, centered at the retrieval mean) retrieved over the subregion by CALIPSO is plotted in Figure 8 as the horizontal solid line. Once more, the CALIPSO retrievals are taken from the Version 3 level 2 5 km Cloud Layer product, and are those in which the CALIPSO cloud profiles are not totally attenuated. Also plotted, as the dotted horizontal line, is the range of 1.38 μm retrieved optical thickness for the MODIS pixels nearest the CALIPSO ground track that correspond to the non-totally-attenuating CALIPSO cloud profiles. For this case, the mean of the CALIPSO optical thickness retrievals (78 total pixels, of which only one is constrained) is approximately 0.5, while the 1.38 μm retrieval mean is near 0.9. Unlike Figure 6, however, there is significant overlap between the CALIPSO and MODIS 1.38 μm retrieval ranges.

4. Estimating Retrieval Uncertainty

[35] Quantitative pixel-level baseline retrieval uncertainties, nominally the root-sum-square of various uncertainty

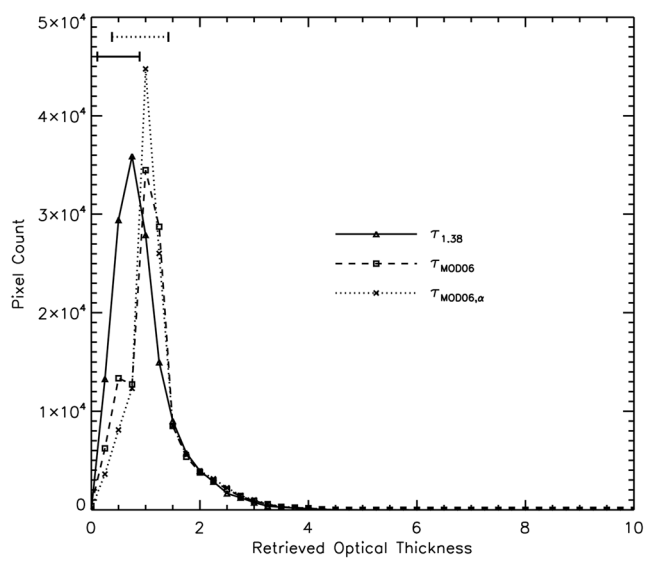

Figure 8. Optical thickness retrieval histograms for the 1.38 μm approach (solid line), operational MOD06 (dashed line), and modified MOD06 (dotted line) for the 9 August 2009 case shown in Figure 7. The modified MOD06 uses the mean Cox-Munk ocean surface albedo (here about 4.6%). The horizontal solid and dotted lines denote the range of optical thickness retrieved by CALIPSO (Version 3 level 2 5 km Cloud Layer product) and the 1.38 μm approach (nearest pixels to CALIPSO ground track), respectively.

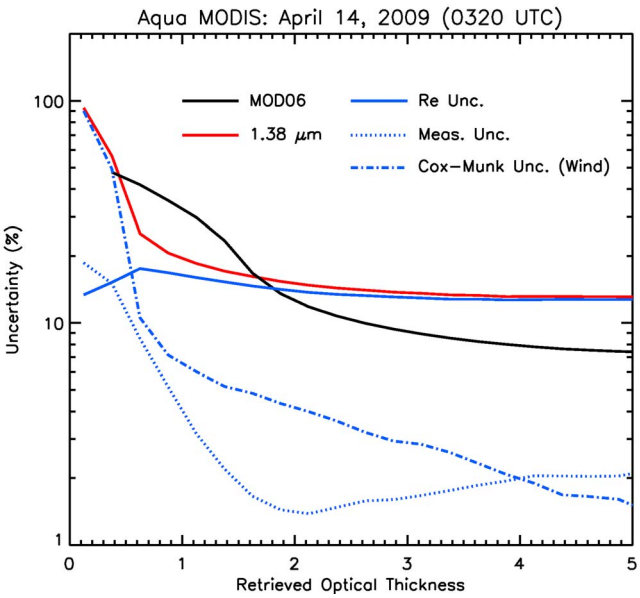

Figure 9. Estimated baseline retrieval uncertainty for the 1.38 μm retrieval (red line) and MOD06 (black line) corresponding to the red outlined region in the 14 April case (Figure 5a), plotted with respect to optical thickness. In addition, the 1.38 μm retrieval uncertainty has been separated into its components: estimated uncertainty due to effective size assumptions (solid blue line), MODIS instrument uncertainty (dotted blue line), and uncertainty due to surface assumptions (dash-dotted blue line).

components, for MOD06 were reported for the first time in the Collection 5 reprocessing stream [*Platnick et al.*, 2004]. Three independent error sources are accounted for, namely, measurement (i.e., instrument calibration and plane-parallel LUT models), above-cloud atmospheric transmittance, and surface albedo. Here a similar technique is used to estimate the pixel-level retrieval uncertainty of the 1.38 μm approach, accounting for error sources including measurement and surface albedo, in addition to the added uncertainty due to the particle effective size sensitivity (atmospheric transmittance uncertainty, adding a negligible 1% or less to the total uncertainty, is ignored).

[36] For each error source, a standard deviation has been defined corresponding to its relative uncertainty. For instance, considering measurement uncertainty ($\sigma_{\Delta R}$), the assigned UI value of each MODIS pixel can be directly converted to the relative (%) reflectance uncertainty [*Xiong et al.*, 2005], such that

$$uncertainty(\%) = specified_uncertainty * \exp(UI/scaling_factor), \tag{8}$$

where *specified_uncertainty* and *scaling_factor* refer to constants specified for each MODIS channel within the Level-1b file. For surface albedo, the Cox-Munk uncertainty ($\sigma_{\Delta\alpha}$) can be determined from wind speed uncertainty, which is estimated using the QuikSCAT mission requirements (2 m s^{-1} for wind speed between 3 and 20 m s^{-1}, 10% for wind speed between 20 and 30 m s^{-1}) [*Callahan*, 2006]. Admittedly, using the QuikSCAT mission requirements may underestimate the actual uncertainty inherent in the NCEP reanalyses; nevertheless, they provide a useful baseline for wind speed uncertainty.

[37] Favoring simplicity at the expense of computational efficiency, for each error source the retrieval is run for both $\pm\sigma$, instead of deriving partial derivatives for the sensitivities. The retrieval uncertainty, $\sigma_{\Delta\tau,k}$, for each error source k is thus defined as the root-mean-square of the retrieved optical thicknesses τ_n ($\tau_{\pm\sigma\ k}$ and the actual retrieved value τ), such that

$$\sigma_{\Delta\tau,k} = \sqrt{\sum\nolimits_{n=1}^{3} \frac{(\tau_n - \overline{\tau}k)^2}{n}}, \tag{9}$$

where $\overline{\tau_k}$ is the mean of τ_n.

[38] Effective radius uncertainty ($\sigma_{\Delta\ \mathrm{Re}}$), however, is estimated in a different manner. Inherent in the 30 μm assumption is an assumed effective radius distribution (i.e., the Aqua MODIS global retrieval distribution). Optical thickness is first retrieved for 10 effective radius values, corresponding to the forward LUT radii between 5 and 50 μm, and a retrieved optical thickness distribution is produced. The retrieval uncertainty due to effective radius uncertainty is thus estimated using the standard deviation derived from the retrieved optical thickness distribution, such that

$$\sigma_{\Delta\tau_{\mathrm{Re}}} = \sqrt{\sum\nolimits_{i=1}^{n_{\mathrm{Re}}} (\tau_i - \mu_\tau)^2 \cdot P(Re_i)} \tag{10a}$$

$$\mu_\tau = \sum\nolimits_{i=1}^{n_{\mathrm{Re}}} \tau_i \cdot P(Re_i), \tag{10b}$$

where τ_i is the optical thickness retrieved corresponding to each forward LUT effective radius Re_i, $P(Re_i)$ is the probability of having effective radius Re_i (derived from the Aqua MODIS global retrieval distribution), μ_τ is the expected value of optical thickness derived from the retrieved optical thickness distribution, and n_{Re} is the number of forward LUT effective radii (here n_{Re} = 10).

[39] The total retrieval uncertainty $\sigma_{\Delta\tau}$ can then be defined, assuming the error sources are uncorrelated, as the root-sum-square of the three error sources, such that

$$\sigma_{\Delta\tau} = \sqrt{\sigma^2_{\Delta\tau_{\mathrm{Re}}} + \sigma^2_{\Delta\tau_R} + \sigma^2_{\Delta\tau_\alpha}}, \tag{11}$$

where $\sigma_{\Delta\tau_{\mathrm{Re}}}$, $\sigma_{\Delta\tau_R}$, and $\sigma_{\Delta\tau_\alpha}$ are the uncertainties due to the effective radius sensitivity, measurement, and surface albedo errors, respectively. Relative uncertainty in percent is subsequently defined as

$$Unc(\%) = \left(\frac{\sigma_{\Delta\tau}}{\tau}\right) \times 100 \tag{12}$$

[40] Figure 9 shows the relative retrieval uncertainties as a function of optical thickness for the red outlined region in the 14 April 2009 case in Figure 5a. Here the solid black and red lines denote the operational MOD06 and 1.38 μm retrieval uncertainties, respectively. Also plotted are uncertainties for the individual 1.38 μm retrieval error sources: effective radius assumption (solid blue line), measurement

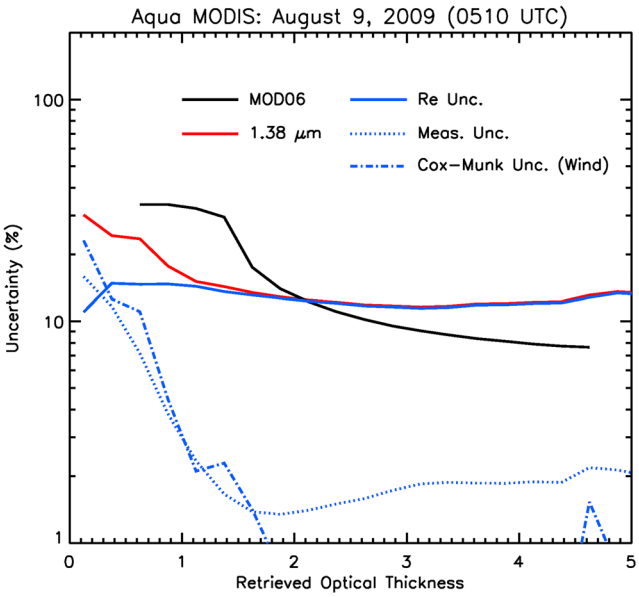

Figure 10. Estimated baseline retrieval uncertainty for the 1.38 μm retrieval (red line) and MOD06 (black line) corresponding to the red outlined region in the 9 August case (Figure 7a), plotted with respect to optical thickness. In addition, the 1.38 μm retrieval uncertainty has been separated into its components: estimated uncertainty due to effective size assumptions (solid blue line), MODIS instrument uncertainty (dotted blue line), and uncertainty due to surface assumptions (dash-dotted blue line). Discontinuities indicate nonretrieved optical thickness values.

(dotted blue line), and Cox-Munk surface albedo (dash-dotted blue line). It is evident that the uncertainty due to the effective radius assumption dominates, with the exception of very small τ (less than 0.5 to 1.0), where measurement and surface albedo uncertainties become quite large. For this case, the MOD06 uncertainty is smaller than the 1.38 μm retrieval uncertainty for τ larger than about 2, then becomes larger for smaller τ. However, MOD06 uncertainty again becomes smaller than the 1.38 μm retrieval around $\tau = 0.5$. Several factors are at play here. First, the operational MOD06 uncertainties assume a constant measurement/model uncertainty of 5%, whereas the present study uses only pixel-level relative measurement uncertainty converted from the UI. Accounting for the pixel-level UI (applicable to other spectral channels) could potentially increase the MOD06 uncertainty at small optical thicknesses. In addition, the operational MOD06 retrievals assume a Lambertian diffuse surface albedo of 5%, with 15% relative uncertainty. It is difficult to project how a Cox-Munk ocean surface assumption would affect MOD06 uncertainties. Using the 1.38 μm Cox-Munk uncertainty as a guide, however, indicates that MOD06 uncertainties could dramatically increase for small τ.

[41] Figure 10 shows the relative retrieval uncertainties for the red outlined region in the 8 August 2009 case in Figure 7a. Again, the solid black and red lines denote the operational MOD06 and 1.38 μm total retrieval uncertainties, respectively, while the blue lines denote the individual 1.38 μm retrieval error sources. As in Figure 9, the effective radius assumption dominates the 1.38 μm retrieval uncertainties, except at small optical thickness. In addition, the MOD06 uncertainties are smaller than the 1.38 μm uncertainties for thicker clouds, but become larger for clouds with τ less than about 2. However, unlike the 14 April case, the 1.38 μm retrieval uncertainties appear to remain smaller than those of MOD06 for all τ less than 2. Once more, the MOD06 uncertainties potentially could be larger if measurement uncertainties are defined with appropriate UIs, as well as with the implementation of a Cox-Munk ocean surface BRDF.

5. Summary and Conclusions

[42] The 1.38 μm channel has been shown to be quite useful for thin cirrus cloud detection [*Gao et al.*, 1993] due to its location in a strong water vapor absorption band. This unique characteristic, however, results in nonnegligible attenuation in satellite-observed 1.38 μm cloud reflectances, a consequence of the small amount of atmospheric water vapor located above and within the cirrus layer. As a result, quantifying derived optical thickness and its uncertainty is problematic. Here a new technique has been developed to estimate the above/in-cloud water vapor attenuation at 1.38 μm, and to subsequently retrieve thin cirrus cloud optical thickness, with the intention to supplement MOD06 for cases in which the operational cloud retrieval algorithms fail. This technique pairs the 1.24 μm channel with 1.38 μm to estimate the water vapor transmittance from the slope calculated from the cloudy reflectance observations and estimated clear-sky reflectances. This channel pairing was selected due to the close spectral proximity (and, thus, similar ice cloud scattering properties) of the 1.24 μm channel to 1.38 μm, which acts to minimize the particle effective size sensitivity of the retrieval.

[43] At present, the retrieval is limited to ocean cases only, where atmospheric water vapor content is generally large and the surface at 1.24 μm is relatively dark. To more realistically capture ocean surface reflection, a Cox-Munk approach is used to define the ocean surface BRDF, from which the clear-sky reflectance at 1.24 μm is estimated. The retrieval is shown to perform well, retrieving up to 38% more pixels than MOD06 for the case studies shown here. Baseline retrieval uncertainties are dominated by the particle effective size assumption for moderately thick cirrus ($\tau > 1$), and are estimated to be between 15 and 20% (corresponding MOD06 uncertainties are around 10%). For thin cirrus ($\tau < 1$), where the surface assumption becomes dominant, baseline uncertainties can vary widely depending on the proximity to the Sun glint region; here they are estimated to be near 30% and 90% for the two case studies (corresponding MOD06 uncertainties are near 35% and 50%, respectively). While operational MOD06 uncertainties for thin cirrus are in fact smaller for the 14 April 2009 case study, it should be noted that, in addition to using a Cox-Munk approach to estimate ocean surface BRDF (whereas MOD06 assumes a Lambertian surface with 5% albedo), the 1.38 μm retrieval uses the Level-1b UI to define pixel-level measurement uncertainty (in contrast, MOD06 assumes a constant 5% uncertainty). Figures 9 and 10 indicate that using both a Cox-Munk assumption and UI-defined measurement uncertainty in MOD06 is likely to increase retrieval

uncertainty for small optical thicknesses, although the magnitude of such an increase is at present unknown. Note that an analysis of including such assumptions in the next collection of MOD06 processing is currently ongoing.

[44] While the case studies highlighted here show an impressive increase in cirrus retrievals, it is unclear to what extent this translates to increased retrievals over much larger regions. Subsequently, further investigation will be required to fully address the impacts of the 1.38 μm retrieval on the spatial and temporal MOD06 cloud global and regional statistics (i.e., global Level-3 gridded statistics), in addition to the resulting impacts on MOD06-derived cloud radiative effects. Nevertheless, because next-generation sensors such as VIIRS and GOES-R, among others, will include the 1.38 μm channel, the present technique should prove to be useful into the future.

[45] **Acknowledgments.** This research was supported by an appointment to the NASA Postdoctoral Program, administered by Oak Ridge Associated Universities through a contract with NASA, at the Goddard Space Flight Center, and by MODIS science team funding from NASA. In addition, the authors wish to thank Zhibo Zhang for his generous assistance and many helpful suggestions during the course of this work and Tom Arnold for his development of and assistance with the MODIS imaging software.

References

Ackerman, S. A., R. E. Holz, R. Frey, E. W. Eloranta, B. C. Maddux, and M. McGill (2008), Cloud detection with MODIS. Part II: Validation, *J. Atmos. Oceanic Technol.*, *25*, 1073–1086, doi:10.1175/2007JTECHA1053.1.

Austin, R. T., A. J. Heymsfield, and G. L. Stephens (2009), Retrieval of ice cloud microphysical parameters using the CloudSat millimeter-wave radar and temperature, *J. Geophys. Res.*, *114*, D00A23, doi:10.1029/2008JD010049.

Baum, B. A., D. P. Kratz, P. Yang, S. C. Ou, Y. Hu, P. Soulen, and S. C. Tsay (2000), Remote sensing of cloud properties using MODIS airborne simulator imagery during SUCCESS: 1. Data and models, *J. Geophys. Res.*, *105*, 11,767–11,780, doi:10.1029/1999JD901089.

Baum, B. A., A. J. Heymsfield, P. Yang, and S. T. Bedka (2005a), Bulk scattering properties for the remote sensing of ice clouds. Part I: Microphysical data and models, *J. Appl. Meteorol.*, *44*, 1885–1895, doi:10.1175/JAM2308.1.

Baum, B. A., P. Yang, A. J. Heymsfield, S. Platnick, M. D. King, Y.-X. Hu, and S. T. Bedka (2005b), Bulk scattering properties for the remote sensing of ice clouds. Part II: Narrowband models, *J. Appl. Meteorol.*, *44*, 1896–1911, doi:10.1175/JAM2309.1.

Buriez, J. C., C. Vanbauce, F. Parol, P. Goloub, M. Herman, B. Bonnel, Y. Fouquart, P. Couvert, and G. Seze (1997), Cloud detection and derivation of cloud properties from POLDER, *Int. J. Remote Sens.*, *18*, 2785–2813, doi:10.1080/014311697217332.

Callahan, P. S. (2006), QuikSCAT science data product user's manual: Overview and geophysical data products, V3.0, *D-18053-RevA*, JPL, Pasadena, Calif.

Cox, C., and W. Munk (1954a), Measurements of the roughness of the sea surface from photographs of the Sun's glitter, *J. Opt. Soc. Am.*, *44*, 838–850, doi:10.1364/JOSA.44.000838.

Cox, C., and W. Munk (1954b), Statistics of the sea surface derived from Sun glitter, *J. Mar. Res.*, *13*, 198–227.

Dessler, A. E., and P. Yang (2003), The distribution of tropical thin cirrus clouds inferred from Terra MODIS data, *J. Clim.*, *16*, 1241–1247, doi:10.1175/1520-0442(2003)16<1241:TDOTTC>2.0.CO;2.

Gao, B.-C., A. F. H. Goetz, and W. J. Wiscombe (1993), Cirrus cloud detection from airborne imaging spectrometer data using the 1.38 μm water vapor band, *Geophys. Res. Lett.*, *20*, 301–304, doi:10.1029/93GL00106.

Gao, B.-C., Y. J. Kaufman, W. Han, and W. J. Wiscombe (1998), Correction of thin cirrus path radiances in the 0.4–1.0 μm spectral region using the sensitive 1.375 μm cirrus detecting channel, *J. Geophys. Res.*, *103*, 32,169–32,176, doi:10.1029/98JD02006.

Gao, B.-C., P. Yang, W. Han, R.-R. Li, and W. J. Wiscombe (2002), An algorithm using visible and 1.38-μm channels to retrieve cirrus cloud reflectances from aircraft and satellite data, *IEEE Trans. Geosci. Remote Sens.*, *40*, 1659–1668, doi:10.1109/TGRS.2002.802454.

Holz, R. E., S. A. Ackerman, F. W. Nagle, R. Frey, S. Dutcher, R. E. Kuehn, M. A. Vaughan, and B. Baum (2008), Global Moderate Resolution Imaging Spectroradiometer (MODIS) cloud detection and height evaluation using CALIOP, *J. Geophys. Res.*, *113*, D00A19, doi:10.1029/2008JD009837.

Jensen, E., and L. Pfister (2005), Implications of persistent ice supersaturation in cold cirrus for stratospheric water vapor, *Geophys. Res. Lett.*, *32*, L01808, doi:10.1029/2004GL021125.

Kahn, B. H., C. K. Liang, A. Eldering, A. Gettelman, Q. Yue, and K. N. Liou (2008), Tropical thin cirrus and relative humidity observed by the Atmospheric Infrared Sounder, *Atmos. Chem. Phys.*, *8*, 1501–1518, doi:10.5194/acp-8-1501-2008.

King, M. D., S.-C. Tsay, S. E. Platnick, M. Wang, and K.-N. Liou (1998), Cloud retrieval algorithms for MODIS: Optical thickness, effective particle radius, and thermodynamic phase, *ATBD-MOD-05*, NASA Goddard Space Flight Cent., Greenbelt, Md.

King, M. D., S. Platnick, P. A. Hubanks, G. T. Arnold, E. G. Moody, G. Wind, and B. Wind (2006), Collection 005 change summary for the MODIS cloud optical property (06_OD) algorithm, report, NASA Goddard Space Flight Cent., Greenbelt, Md.

King, M. D., S. Platnick, G. Wind, G. T. Arnold, and R. T. Dominguez (2010), Remote sensing of radiative and microphysical properties of clouds during TC4: Results from MAS, MASTER, MODIS, and MISR, *J. Geophys. Res.*, *115*, D00J07, doi:10.1029/2009JD013277.

Kou, L., D. Labrie, and P. Chylek (1993), Refractive indices of water and ice in the 0.65- to 2.5-μm spectral range, *Appl. Opt.*, *32*, 3531–3540, doi:10.1364/AO.32.003531.

Kratz, D. P. (1995), The correlated k-distribution technique as applied to the AVHRR channels, *J. Quant. Spectrosc. Radiat. Transfer*, *53*, 501–517, doi:10.1016/0022-4073(95)00006-7.

Lee, J., P. Yang, A. Dessler, B.-C. Gao, and S. Platnick (2009), Distribution and radiative forcing of tropical thin cirrus clouds, *J. Atmos. Sci.*, *66*, 3721–3731, doi:10.1175/2009JAS3183.1.

Mace, G. G., Y. Zhang, S. Platnick, M. D. King, P. Minnis, and P. Yang (2005), Evaluation of cirrus cloud properties derived from MODIS data using cloud properties derived from ground-base observations collected at the ARM SGP site, *J. Appl. Meteorol.*, *44*, 221–240, doi:10.1175/JAM2193.1.

Macke, A., M. I. Mishchenko, and B. Cairns (1996a), The influence of inclusions on light scattering by large ice particles, *J. Geophys. Res.*, *101*, 23,311–23,316, doi:10.1029/96JD02364.

Macke, A., J. Mueller, and E. Raschke (1996b), Single scattering properties of atmospheric ice crystal, *J. Atmos. Sci.*, *53*, 2813–2825, doi:10.1175/1520-0469(1996)053<2813:SSPOAI>2.0.CO;2.

Meyer, K., P. Yang, and B.-C. Gao (2004), Optical thickness of tropical cirrus clouds derived from the MODIS 0.66- and 1.375-μm channels, *IEEE Trans. Geosci. Remote Sens.*, *42*, 833–841, doi:10.1109/TGRS.2003.818939.

Meyer, K., P. Yang, and B.-C. Gao (2007), Ice cloud optical depth from MODIS cirrus reflectance, *IEEE Geosci. Remote Sens. Lett.*, *4*, 471–474, doi:10.1109/LGRS.2007.897428.

Oreopoulos, L., S. E. Platnick, G. Hong, P. Yang, and R. F. Cahalan (2009), The shortwave radiative forcing bias of homogeneous liquid and ice clouds observed by MODIS, in *Current Problems in Atmospheric Radiation (IRS 2008)*, edited by T. Nakajima and M. A. Yarnasoe, pp. 569–572, AIP, Melville, N. Y.

Platnick, S., M. D. King, S. A. Ackerman, W. P. Menzel, B. A. Baum, J. C. Riedi, and R. A. Frey (2003), The MODIS cloud products: Algorithms and examples from Terra, *IEEE Trans. Geosci. Remote Sens.*, *41*, 459–473, doi:10.1109/TGRS.2002.808301.

Platnick, S., R. Pincus, B. Wind, M. D. King, M. Gray, and P. Hubanks (2004), An initial analysis of the pixel-level uncertainties in global MODIS cloud optical thickness and effective particle size retrievals, *Proc. SPIE Int. Soc. Opt. Eng.*, *5652*, doi:10.1117/12.578353.

Roskovensky, J. K., and K. N. Liou (2003), Detection of thin cirrus using a combination of 1.38-μm reflectance and window brightness temperature difference, *J. Geophys. Res.*, *108*(D18), 4570, doi:10.1029/2002JD003346.

Schmidt, K. S., V. Venema, F. Di Giuseppe, R. Scheirer, M. Wendisch, and P. Pilewskie (2007), Reproducing cloud microphysical and irradiance measurements using three 3D cloud generators, *Q. J. R. Meteorol. Soc.*, *133*, 765–780, doi:10.1002/qj.53.

Schmidt, K. S., G. Feingold, P. Pilewskie, H. Jiang, O. Coddington, and M. Wendisch (2009), Irradiance in polluted cumulus fields: Measured and modeled cloud-aerosol effects, *Geophys. Res. Lett.*, *36*, L07804, doi:10.1029/2008GL036848.

Sherwood, S. C. (2002), Aerosols and ice particle size in tropical cumulonimbus, *J. Clim.*, *15*, 1051–1063, doi:10.1175/1520-0442(2002)015<1051:AAIPSI>2.0.CO;2.

Stamnes, K., S.-C. Tsay, W. Wiscombe, and K. Jayaweera (1988), A numerically stable algorithm for discrete-ordinate-method radiative transfer in multiple scattering and emitting layered media, *Appl. Opt.*, *27*, 2502–2509, doi:10.1364/AO.27.002502.

Wind, G., S. Platnick, M. D. King, P. A. Hubanks, M. J. Pavolonis, A. K. Heidinger, P. Yang, and B. A. Baum (2010), Multilayer cloud detection with the MODIS near-infrared water vapor absorption band, *J. Appl. Meteorol. Climatol.*, *49*, 2315–2333, doi:10.1175/2010JAMC2364.1.

Winker, D. M., M. A. Vaughan, A. Omar, Y. Hu, K. A. Powell, Z. Liu, W. H. Hunt, and S. A. Young (2009), Overview of the CALIPSO mission and CALIOP data processing algorithms, *J. Atmos. Oceanic Technol.*, *26*, 2310–2323, doi:10.1175/2009JTECHA1281.1.

Xie, Y., P. Yang, G. W. Kattawar, P. Minnis, and Y. X. Hu (2009), Effect of the inhomogeneity of ice crystals on retrieving ice cloud optical thickness and effective particle size, *J. Geophys. Res.*, *114*, D11203, doi:10.1029/2008JD011216.

Xiong, J., G. Toller, V. Chiang, J. Sun, J. Esposito, and W. Barnes (2005), MODIS level 1b algorithm theoretical basis document, *ATBD-MOD-02*, NASA Goddard Space Flight Cent., Greenbelt, Md.

Yang, P., K. N. Liou, K. Wyser, and D. Mitchell (2000), Parameterization of the scattering and absorption properties of individual ice crystals, *J. Geophys. Res.*, *105*, 4699–4718, doi:10.1029/1999JD900755.

Young, S. A., D. M. Winker, M. A. Vaughan, Y. Hu, and R. E. Kuehn (2008), CALIOP algorithm theoretical basis document, part 4: Extinction retrieval algorithms, *PC-SCI-202 Part 4*, NASA Goddard Space Flight Cent., Greenbelt, Md.

K. Meyer and S. Platnick, NASA Goddard Space Flight Center, Code 613.2, Greenbelt, MD 20771, USA. (kerry.meyer@nasa.gov)